



## SELECTIVE ELECTROCHEMICAL REDUCTION OF CO<sub>2</sub> TO HIGH VALUE CHEMICALS

**Grant agreement no.: 851441**

**Start date:** 01.01.2020 – **Duration:** 36 months

**Project Coordinator:** Dr. Brian Seger - DTU

### DELIVERABLE REPORT

<b>D2.2 PATHWAYS TOWARDS CO, ETHYLENE, ETHANOL ON CU FACETS</b>		
Due Date	Jun. 30, 2021	
Author (s)	Georg Kastlunger (Postdoc) and Karen Chan	
Workpackage	7	
Workpackage Leader	Sophia Haussener	
Lead Beneficiary	DTU-Th	
Date released by WP leader	15-06-2021	
Date released by Coordinator	16-06-2021	
<b>DISSEMINATION LEVEL</b>		
<b>PU</b>	Public	<b>X</b>
<b>PP</b>	Restricted to other programme participants (including the Commission Services)	
<b>RE</b>	Restricted to a group specified by the consortium (including the Commission Services)	
<b>CO</b>	Confidential, only for members of the consortium (including the Commission Services)	
<b>NATURE OF THE DELIVERABLE</b>		
<b>R</b>	Report	<b>X</b>
<b>P</b>	Prototype	
<b>D</b>	Demonstrator	
<b>O</b>	Other	

<b>SUMMARY</b>	
<b>Keywords</b>	<i>CO(2) reduction, Reaction mechanism, DFT, selectivity</i>
<b>Abstract</b>	This deliverable reports on density functional theory (DFT) based analysis on the mechanism of CO(2) reduction towards ethylene and ethanol. Both a thermodynamic assessment and a kinetic analysis have been performed. We identified the rate limiting step shared by the products as the dimerization of two *CO molecules and its reaction to the applied potential. We propose the selectivity determining steps between ethylene and ethanol as the competition between two protonation reactions of HCCO*. This result is consistent with the dependence of ethylene vs. oxygenated products on potential observed in existing experimental studies. For further validation of the computed mechanism, experimental studies on the basis of kinetic isotope effects are planned in collaboration with WP3.
<b>Public abstract for confidential deliverables</b>	

<b>REVISIONS</b>			
<b>Version</b>	<b>Date</b>	<b>Changed by</b>	<b>Comments</b>
<b>0.1</b>	1/06/2021	K. Chan	Initial version from G. Kastlunger
<b>0.2</b>		Sophia Haussener and Etienne Boutin	EPFL Feedback
<b>0.3</b>		Brian Seger	Consortium leader feedback

## 1 INTRODUCTION AND SCOPE

This deliverable reports on the first principle assessment of the mechanisms in CO<sub>2</sub> reduction (CO<sub>2</sub>R) with a special focus on the product selectivity between the major C<sub>2</sub> products, ethylene and ethanol. Since CO<sub>2</sub> and CO reduction lead to similar activities, we considered CO as the starting point towards these C<sub>2</sub> products. It is an integral part of WP7's modelling efforts by providing an atomistic understanding of the intrinsic reaction mechanisms, which will be integrated into the mass transport models developed in EPFL as effective kinetic expressions. The workhorse for achieving this task was a theoretical assessment on the basis of constant potential density functional theory<sup>1</sup>. Both the thermodynamics on a variety of Cu surface facets of possible reaction intermediates and the kinetics along the most promising reaction pathways have been studied.

The analysis led to the identification of a reasonable reaction mechanism and the identification of the selectivity determining steps towards ethylene, ethanol, acetate and acetaldehyde. We found the potential dependence of oxygenates and hydrocarbons to vary such that oxygenates are favoured at lower overpotentials, while hydrocarbons are favoured at higher ones. This observation was consistent with experimental data from a variety of published experimental data<sup>3</sup>.

On the basis of the theoretical insights and to further evaluate the theoretical model, experiments on the influence of the kinetic isotope effect on selectivity and the production of novel products by cofeeding of reagents have been proposed and will be conducted in collaboration with WP3.

## 2 RESULTS AND DISCUSSION

### 2.1 Thermodynamic assessment of the reaction network to valuable products

We evaluated the thermodynamics of all possible reaction intermediates on the most common metal surfaces on Cu, namely the 111, 100, 110, and 211 facets. As an initial intermediate for this study adsorbed CO (\*CO) has been chosen, given the consensus that it is a common intermediate in CO<sub>2</sub>R and COR preceding the rate limiting step towards multicarbon products and methane. The chosen starting point is further justified by the analysis performed in section 2.4, where we will show that CO<sub>2</sub>R and COR lead to identical activity. We applied the computational hydrogen electrode (CHE) model along with an explicit inclusion of a water layer in the simulation to account for solvation effects. The adsorbates' interaction with an electric field was accounted for by performing all calculations in a grand-canonical framework<sup>1</sup>. We find that the thermodynamics agree qualitatively between the studied facets. Given the large amount of energetically similar intermediates, a study of the reaction kinetics is needed for identifying the actual mechanism.

Figure 1 shows the calculated free energy diagram towards ethylene, ethanol and methane shown for Cu(100) at 0V<sub>RHE</sub> and pH 13. The energetics are representative for the other studied facets, where the relative ordering of intermediates has been found to be comparable. Given the plethora of steps shown in the upper panel of Figure 1 and the size of the possible reaction intermediates, the number of possible reaction pathways is vast. Furthermore, the large cathodic overpotentials applied in CO<sub>2</sub>R lead to the situation where the thermodynamics of the reaction are generally downhill. Hence, from this first study we concluded that an assessment of the reaction kinetics is crucial for identifying the mechanism. We followed two strategies in this scope:

- *Identification of the rate determining step:* It is likely that C<sub>2+</sub> products share a common RDS, given their equal pH dependence and comparable potential dependence. The identification of this step pins down the mechanism up to this point in the reaction network, and substantially narrows down the number of subsequent intermediates
- *Stepwise kinetic analysis of the reaction mechanism:* Starting from the RDS, we studied all the elementary steps leading to later reaction intermediates that arose from our thermodynamic analysis. This strategy allowed us to exclude the formation of kinetically hindered intermediates and made it possible to walk

along the reaction cascade by following the path of the lowest activation energy, which predominates in the reaction rate. In addition, elementary steps starting from the same intermediate with comparable kinetic barriers could be studied in more detail to identify the selectivity determining steps.

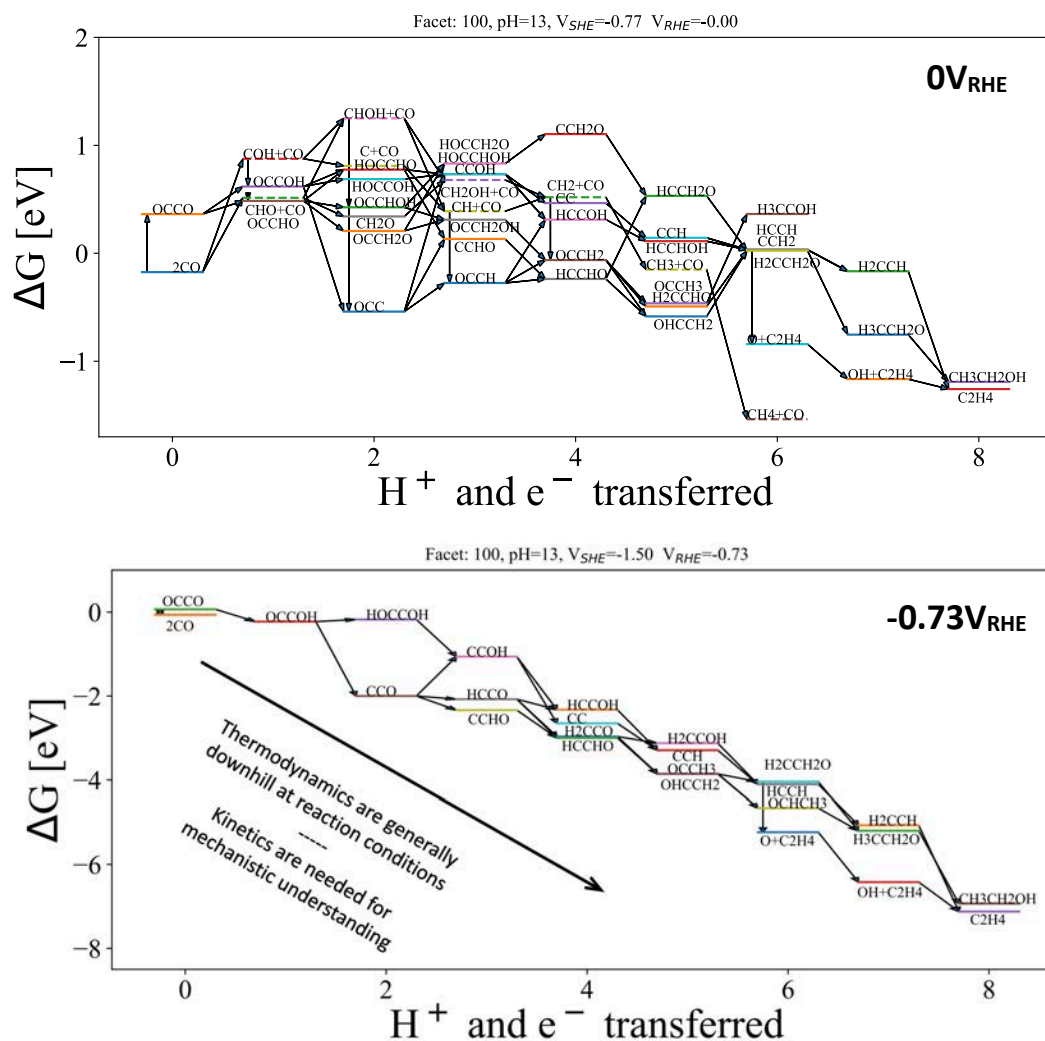


**Figure 1:** Thermodynamic assessment of the possible reaction intermediates in electrochemical CO reduction on Cu(100). Upper panel: Complete investigation on the all possible reaction intermediate at 0V<sub>RHE</sub>. Lower panel: Free energy diagram at reaction conditions, where the number of intermediates has been reduced for clarity.

## 2.2 Identification of the rate limiting step in CO reduction to C2+ products

As a first step to narrow down the possibilities of the reaction mechanisms, we identified the rate determining step (RDS) using simulations of activation energies via the nudged elastic band (NEB) method performed under constant potential<sup>1</sup> at alkaline conditions (where H<sub>2</sub>O is the proton donor). We found that \*CO dimerization is the most likely RDS, while an initial protonation of \*CO is unfavoured. The potential response of COR activity towards C<sub>2</sub>+ products is a consequence of the polarization of the \*OCCO intermediate<sup>2</sup>.

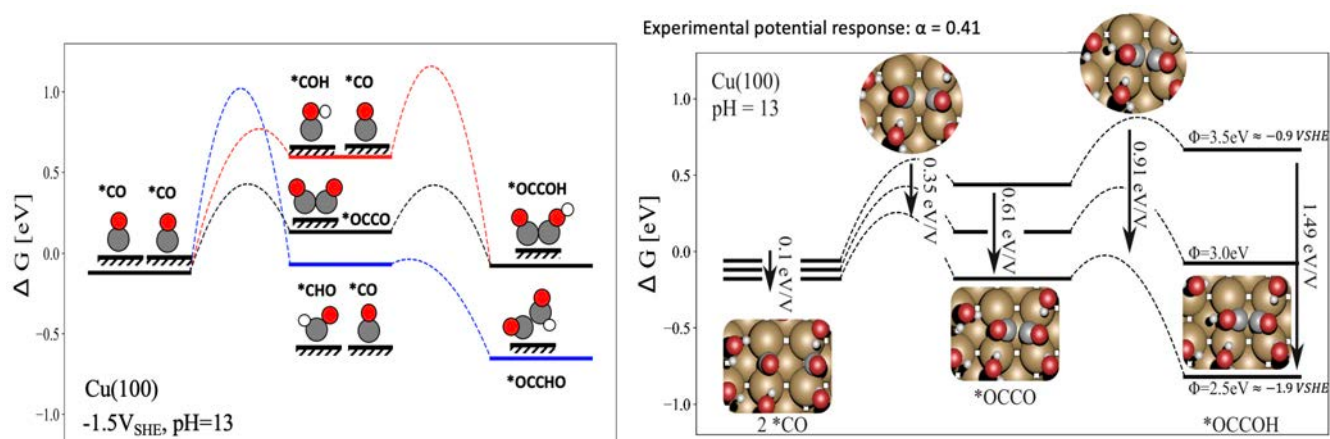


**Figure 2:** a) Free energy diagram for the study of the RDS of COR towards C<sub>2+</sub> products, comparing the mechanism based on initial protonation and \*CO dimerization on the Cu(100) facet. Horizontal lines represent thermodynamically stable reaction intermediates, which are also shown as schematics nearby. The dashed lines represent the reaction barriers of the elementary steps. b) Potential response of the \*CO dimerization mechanism as calculated from DFT. The arrows and nearby labels correspond to the energetic stabilization with cathodic overpotential. The values of the potential response directly translate into Butler-Volmer transfer coefficients of the same value. The insets show an illustration of the geometries of the respective states resulting from the calculations

Given the pH independence of CO<sub>(2)</sub> reduction to C<sub>2+</sub> products, well known in the literature<sup>2</sup>, the position of the RDS needs to be located at the very start of reaction network. Figure 2a shows our results on the possibilities for RDS starting from 2 CO molecules adsorbed on the Cu(100) surface. We calculated the activation energies for an initial protonation (both on C and O of \*CO) and the dimerization of \*CO on all four investigated facets. We found that the dimerization of \*CO on the (100) facets leads to highest activity and is clearly favoured over a protonation at reaction conditions, given its substantially lower free energy barrier, making a coupling of two \*CO at a later stage of the mechanism unlikely.

Following the \*CO dimerization mechanism, the potential response of COR towards C<sub>2+</sub> products does not arise from the classical stabilization of a proton-coupled electron transfer. Instead, the reaction to a change in driving force arises from the polarization of the \*OCCO intermediate, without the need of a proton, cancelling any pH dependence. Figure 2b shows the determined potential response of the reaction intermediates and transition states. We found that the stabilization of the transition state of \*CO dimerization with potential (0.35eV/V) is in reasonable agreement with the experimental Butler-Volmer transfer coefficients of 0.41 for CO<sub>(2)</sub>R to C<sub>2+</sub> products, which we determined from a statistical analysis on the basis of a database of experimental studies created in the course of the work on this work package<sup>3</sup>.

Furthermore, Figure 2b shows that the RDS changes with the applied potential. At high overpotential ( $U_{SHE} < -1.4\text{V}$ ) \*CO dimerization limits the reaction rate, while at less cathodic potentials the protonation of \*OCCO becomes the RDS. We note, however, that this does not mean that at low overpotential a \*OCCO coverage is present. Since the step from 2\*CO to \*OCCO is uphill in free energy, the reaction equilibrium will still favour \*CO. While the absolute value of the potential where the transition in RDS happens is subject to model inaccuracies, the qualitative behaviour is expected. We suggest that the actual potential where the transition in RDS happens could be studied by performing experiments at very low overpotentials on Cu catalysts with high electrochemically active surface area at a range of pH.

Independent of the RDS being \*CO dimerization or the protonation of \*OCCO, the \*CO dimerization pathway mechanism is clearly favoured over one with an initial protonation. We used this finding as a starting point for our investigation of the selectivity determining step (SDS), discussed in the following section.

### 2.3 Identification of the selectivity determining steps towards C2 products

Performing a stepwise kinetic analysis along the reaction network allowed us to narrow down the mechanism towards ethylene, ethanol, acetaldehyde and acetate. Figure 3 shows a schematic of the identified mechanism, which illustrates that all C2 products share a common path until the  $*\text{HCCO}$  intermediate. The protonation of the oxygen end of  $*\text{HCCO}$  leads to ethylene, while the protonation of the terminal C leads to the creation of oxygenated products. The formation of acetate and acetaldehyde happens along the path to ethanol. Thus, the protonation of  $*\text{HCCO}$  is the SDS between ethylene and oxygenates.

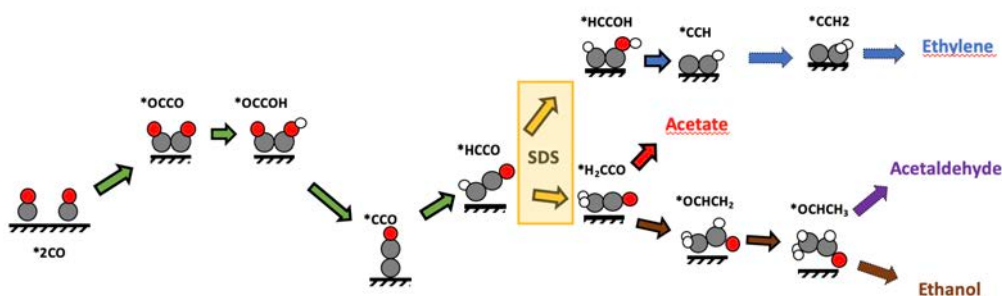


**Figure 3:** Schematic of the reaction mechanisms towards C2 products in COR. Green arrows represent common steps towards all products. Yellow arrows symbolize the SDS between ethylene and the other products. Arrows colored differently represent the path to the product of the respective color.

Figure 4 shows the results from the kinetic analysis of the protonation of  $*\text{HCCO}$  in more detail. As the left panel shows, the activation energies of protonating O (in red) and the terminal C (in black) are close, which allows both reactions to happen. The central panel shows the turnover frequencies for the three reaction intermediates, while the right panel shows the selectivity towards the respective intermediates, defined as

$$S_A = \frac{r_A}{\sum r_i} \quad (1)$$

where  $r_A$  is the turnover frequency towards intermediate A and  $\sum r_i$  is the sum of the turnover frequencies to all possible intermediates. At low overpotentials, the path via ketene ( $*\text{H}_2\text{CCO}$ ) that results from protonation of the terminal C in  $*\text{HCCO}$  (black, middle panel) predominates, which leads to higher selectivity towards oxygenated products. Upon increasing the overpotential, the pathway via  $*\text{HCCOH}$  (red, top panel) is favoured; HCCOH is thermodynamically less stable, but kinetically favoured due to facile protonation of O, and results in the switch in selectivity towards ethylene. The protonation of the central C of the  $*\text{HCCO}$  intermediate (blue, lower panel), which would lead to the thermodynamically most stable  $*\text{OHCCCH}$  intermediate, does not play a role in the mechanism due to its high reaction barrier. This finding highlights the necessity of a kinetic analysis for the identification of reaction mechanisms in electrochemistry, given that a purely thermodynamic treatment would erroneously suggest the path towards  $*\text{OHCCCH}$  to be the most favourable.

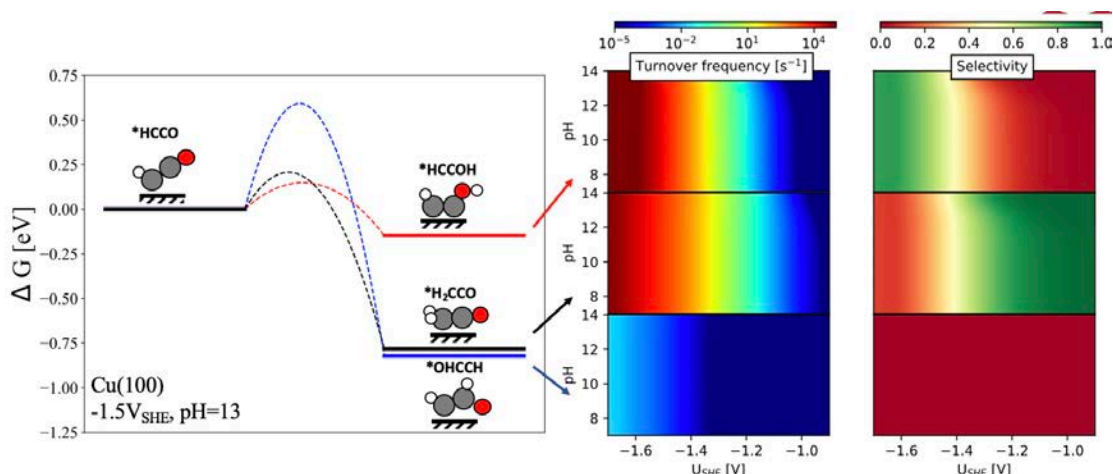


**Figure 4:** Competition towards different products at the identified SDS. The left panel shows the respective activation energies towards the three possible intermediates created from protonating  $*HCCO$ . The central panel shows the simulated turnover frequencies resulting from a microkinetic model. The right panel shows the selectivity towards the three reaction intermediates, calculated from the competition in turnover frequency in the central panel.

Figure 5 shows the dependence of activation energies on potential for the intermediates considered in this analysis. In general, we find that the barriers for protonating O show a larger dependence on overpotential than the protonation of carbon atoms. Therefore, the identified trend is not limited to the selectivity between ethylene and ethanol, but might be applicable to the competition between oxygenated and oxygen free products in general.

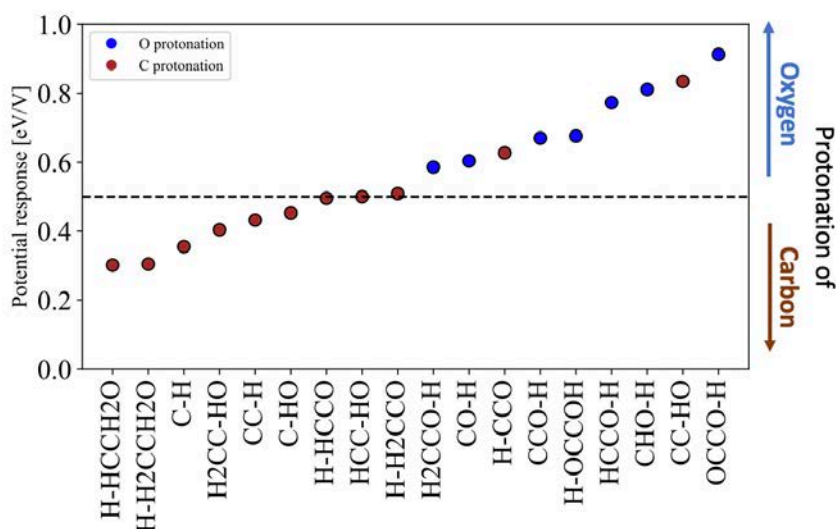


**Figure 5:** Determined potential response of the transition states of protonating a carbon (brown) and oxygen (blue). The “-” sign in the labels represents the bond formed at the transition state.

Upon forming ketene ( $*H_2CCO$ ), acetate can split from the other oxygenates. For this SDS we identified that acetate is formed in solution by a reaction of the closed shell  $H_2CCO_{(aq)}$  molecule with  $OH^-$  from the electrolyte. Note that the corresponding reaction rate of  $H_2CCO_{(aq)}$  with  $H_2O$  is several orders of magnitude smaller, and therefore does not predominate under alkaline conditions.<sup>3</sup> The reaction of  $OH^-$  with a surface intermediate is unlikely since it would be an oxidative process that becomes more favourable under more reducing potentials. The solution reaction with  $H_2CCO_{(aq)}$  creates an unexpected pH dependence for a reduction reaction, where increased electrolyte pH benefits the reaction rate to acetate. Hence, a low roughness of the electrode (preventing  $*H_2CCO$  readsorption) and a high local pH at the electrode surface (benefiting the solution reaction) both promote the formation of acetate.

Acetaldehyde ( $\text{H}_3\text{CCHO}$ ) has been identified as an intermediate towards the production of ethanol. At very low overpotentials, the protonation of  $^*\text{H}_3\text{CCHO}$  is hindered and the adsorbate desorbs as a final product. Upon increasing the cathodic potential, the selectivity towards ethanol with respect to  $\text{H}_3\text{CCHO}$  increases drastically, by giving the protonation the driving force it needs for further reduction. This trend is an example of the selectivity behaviour that results from the competition of a chemical (desorption of  $^*\text{H}_3\text{CCHO}$ ) and an electrochemical (protonation of  $^*\text{H}_3\text{CCHO}$ ) elementary step, where the lack of response of the chemical step to the overpotential leads to the disappearance of the corresponding product at high overpotentials.

## 2.4 Evaluation of the computed mechanism vs. experimental data

In order to evaluate the computed mechanism against experiments, we compiled a database of reported  $\text{CO}_{(2)}\text{R}$  experiments. Figure 6 shows the current densities reported by published  $\text{CO}_{(2)}\text{R}$  experiments<sup>4</sup>. The  $\text{CO}_2\text{R}$  and COR data mostly overlap, which allows us to use both sets of data in this analysis of the activity towards the varying products. Acetate shows a wider spread in the data, as a consequence of the pH dependence discussed above. Panel (d) shows the selectivity of ethylene vs. acetate and ethanol (the major oxygenated products), obtained by applying equation (1) on the overall fits shown as a black line in the respective panels (a)-(c). In agreement with the theoretical conclusions, ethanol and acetate govern the product distribution at low overpotential, while at increased cathodic potentials ethylene takes over.

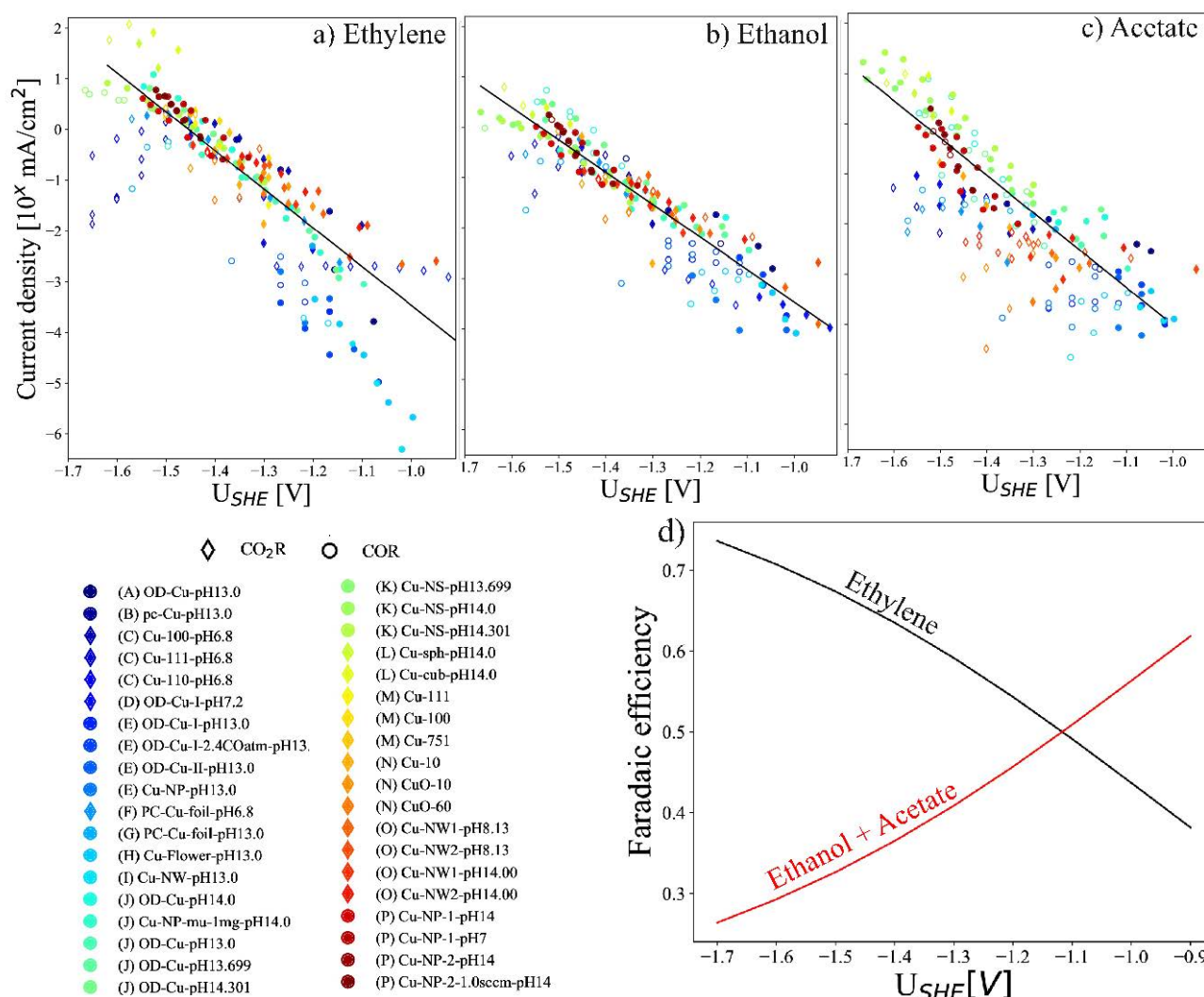


**Figure 6:**  $\text{CO}_{(2)}\text{R}$  activity database for Ethylene, Ethanol and Acetate and the relative faradaic efficiencies towards ethylene and the other products at varying potentials<sup>3</sup>. All currents have been corrected for the electrochemically active surface area (ECSA). Open markers represent mass transport limited points, which have not been included in the fit over all the data shown as a

black line. Acetaldehyde was not included, since no statistically significant amount of data could be retrieved from the literature.

### 3 CONCLUSIONS AND FUTURE WORK

The following recommendations towards the investigated  $C_2$  products of  $CO_{(2)}R$  can be drawn from the identified mechanism:

**Ethylene:** The ethylene pathway splits off upon protonation of  $*HCCO$  (marked as SDS in Figure 3). Its selectivity increases from high overpotentials due to the stronger stabilization of the protonation of the oxygen end of  $*HCCO$ .

**Acetate:** The acetate pathway splits off from the Ethanol/Acetaldehyde path. Its mechanism consists of nucleophilic attack of on desorbed  $*H_2CCO$ , which is promoted with low overpotentials, high pH and low roughness of the catalyst.

**Acetaldehyde:** Acetaldehyde competes only with ethanol and is produced via desorption rather than protonation of adsorbed  $*OCHCH_3$ . Hence, its selectivity is enhanced by low overpotentials and improved mass transport.

**Ethanol:** If the protonation of acetaldehyde is facile, ethanol is produced. Hence ethanol is promoted by intermediate overpotentials and poor mass transport in the experimental setup.

Future work will consist of extending the kinetic analysis to Cu facets beyond the four studied in this deliverable (111, 100, 110, 211.). From the kinetic analysis on the RDS of the reaction, the (100) facet has been identified as most active between the four. Hence, stepped surface facets combining the geometric motif of (100) and an increased binding energy on undercoordinated surface atoms will be studied in more detail.

Furthermore, in order to validate the proposed mechanism, experiments of the effect of kinetic isotopes on the selectivity of  $C_{2+}$  products will be done in the group of Brian Seger (WP3 leader, DTU-Ex). Finally, the identified reaction mechanism leading to acetate opens up the route for a variety of chemical reactions. In a collaboration with the Burdyny group (WP4 leader, Delft), the co-feeding of nucleophilic molecules is expected to allow the production of novel  $CO_{(2)}R$  products, extending the already widespread product possibilities of the reaction.

### 4 REFERENCES

- 1) Kastlunger et al, JPCC 122 (24) 12771-12781 (2018)
- 2) Ringe S. et al, Energy Environ. Sci.,12, 3001-3014 (2019)
- 3) Andraos and Kredge, Can. J. Chem. 78, 508–515 (2000)
- 4) Nitopi et al, Chem. Rev. 119 (12), 7610–7672 (2019)
- 5) Experimental data collection:
  - (A) Bertheussen et al, Angew.Chem. Int.Ed. 55,1450 –1454, (2016)
  - (B) Betheussen et al, ACS Energy Lett. 3, 3, 634–640 (2018)
  - (C) Huang, et al, ACS Catal. 7, 1749–1756 (2017)
  - (D) Li and Kanan, J. Am. Chem. Soc. 134, 17, 7231–7234 (2012)
  - (E) Li et al, Nature 508, 504–507 (2014)
  - (F) Kuhl et al., Energy Environ. Sci. 5, 7050 (2012)
  - (G) Wang et al., ACS Catal. 8, 8, 7445–7454 (2018)
  - (H) Wang et al., Nature Catalysis 2, 702–708 (2019)



- (I) Raciti et al., ACS Catal. 7, 7, 4467–4472 (2017)
- (J) Jouny et al, Nature Catalysis 1, 748–755 (2018)
- (K) Luc et al, Nature Catalysis 2, 423–430 (2019)
- (L) De Gregorio et al, ACS Catal. 10, 9, 4854–4862 (2020)
- (M) Hahn et al, PNAS 114 (23), 5918-5923 (2017)
- (N) Ren et al, Nature Comm. 9, 925, (2018)
- (O) Zhang et al., J. Mater. Chem. A, 7, 26285-26292 (2019)
- (P) Ripatti et al., Joule 3, 240–256 (2019)